Applications of Conformal Mappings

M2R Project, Department of Mathematics

Group AO4

Student Names:

Siddartha Nath, Aya Hayakawa, Kevin Jaku,
Po-Chang Lu, and Tom Goacher

Supervisor:

Professor Darren Crowdy

Submission Date:

June 16th 2020

Imperial College
London

Contents

1 Introduction

Conformal mapping is an important idea in Complex Analysis that has been applied in various fields. What makes this such a useful tool is that it has the following properties:

- Harmonicity is invariant under conformal mapping (Theorem 3.1 on page 4)
- Conformal mapping locally preserves angles and therefore local shapes (Theorem 3.2 on page 4)

The history of conformal mapping dates back to around 150 A.D. when Ptolemy introduced stereographic projection to study the celestial bodies. It was also used later by Kremer to produce the first world map. Since then, up until the nineteenth century, the theoretical side of conformal mapping was established and developed by mathematicians such as Lambert, Gauss, Riemann, and Schwarz. During this period, Riemann published his PhD thesis where the Riemann Mapping Theorem - one of the most important theorems in Complex Analysis to this day - was first introduced. The first numerical study of conformal mapping was done in 1891 and the practical applications of conformal mapping continue to progress and develop further. [1] [2]

The applications in Fluid Flow and Medical Imaging were chosen to be discussed in this report to demonstrate the diversity of disciplines that the technique of conformal mapping has been applied to.

The applications in Fluid Flow are more traditional. Conformal mapping simplifies the situations and problems in this area that are analytically complicated. This is possible because the equations related to Fluid Flow are harmonic (i.e. satisfy Laplace's equation) and remain harmonic after being conformally mapped. Additionally, the local angles of the flows are also preserved under the process.

In Medical Imaging, which is known to be more modern, the algorithms supported by conformal mapping can simplify 3D anatomical structures geometrically, thereby assisting the process of analysis and diagnosis. This is only possible because conformal maps preserve angles and thus preserve local shapes. In both cases, conformal mapping provides good alternatives to methods that are otherwise numerically difficult.

2 Report Overview

This report is strongly related to the Complex Analysis module (MATH95007) and Metric Spaces & Topology module (MATH95008) and focuses on two main applications of conformal mapping:

- Fluid Flow
- Medical Imaging

Chapter 3 introduces some mathematical ideas in Complex Analysis and Metric Spaces & Topology.

Chapter 4 focuses on applications to Fluid Flow, which represent more traditional applications of conformal mappings, where the main focus is on interior corner flows and flows around an airfoil.

Chapter 5 focuses on applications in Medical Imaging, which is a modern application of conformal mappings, where the main focus is on methods surrounding Virtual Colonoscopy.

Chapter 6 contains the conclusion and covers evaluation and possible extensions of this project.

Chapter 7 contains an appendix including: maps, algorithms, and MATLAB codes that are used in this report.

3 Prior Knowledge

A complex function f is said to be conformal in an open set $\Omega \subset \mathbb{C}$ if it is holomorphic in Ω and if $f'(z) \neq 0$, $\forall z \in \Omega$. [3]

Some of the primitive examples of conformal mappings are:

$$w = f(z) = e^z$$

which is conformal everywhere in $\mathbb{C}$ as $f'(z) \neq 0, \forall z \in \mathbb{C}$.

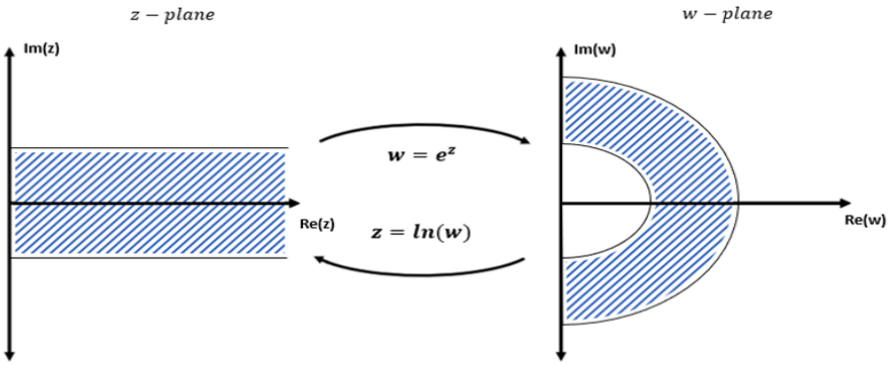

Figure 1: Visual representation of the map $w = e^z$ and its inverse $z = ln(w)$

and

$$w = f(z) = z^2$$

which is conformal in $\mathbb{C} \setminus \{0\}$ as $f'(z) \neq 0, \forall z \in \mathbb{C} \setminus \{0\}$.

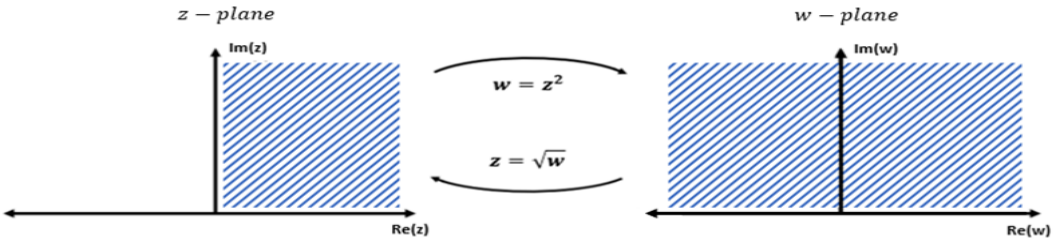

Figure 2: Visual representation of the map $w = z^2$ and its inverse $z = \sqrt{w}$

One way to understand conformal mapping is through its role in giving a geometric interpretation to an analytic function.

This section covers some of the key facts and properties related to conformal mapping that are particularly useful in this report.

3.1 Definitions and Theorems

Definition 3.1 (Analyticity)**.** A complex function is analytic if and only if it is holomorphic. [4]

Thus, the terms "analytic" and "holomorphic" are used interchangeably in this report.

Definition 3.2 (Harmonicity)**.** Let $\phi = \phi(x, y)$ be a real function of two variables $x, y \in \mathbb{R}$. ϕ is harmonic in an open set $\Omega \subset \mathbb{R}^2$ if it satisfies the Laplace's equation (Subsection 3.2.2). [5]

Definition 3.3 (Harmonic Conjugate)**.** Let u be harmonic in an open set $\Omega \subset \mathbb{C}$. Then, there exists a harmonic function v such that $f = u + iv$ is holomorphic in Ω. v is called harmonic conjugate to u. [5]

Theorem 3.1 (Invariance of harmonicity under conformal mappings)**.** *Let $f : \Omega_1 \to \Omega_2$ be conformal and let ϕ be the real part of a holomorphic function g on Ω_2. (i.e. $g = \phi + i\psi$). Then, $\phi \circ f$ is harmonic on Ω_1. (i.e. $\Delta(\phi \circ f) = 0$, where ψ is another real function) [6]*

This is one of the fundamental properties that govern many of the traditional applications of conformal mappings. It aids the construction of solutions to the Laplace's equation obtained in analysing physical phenomena and characteristics including those in aerodynamics, fluid mechanics, and elasticity.

Theorem 3.2 (Angle Preservation Theorem)**.** *Let f be holomorphic in an open subset $\Omega \subset \mathbb{C}$. Suppose that two curves $\gamma_1 = z_1(t)$ and $\gamma_2 = z_2(t)$ lie inside Ω, $t \in [0, 1]$. Assume they intersect at $z_0 = z_1(0) = z_2(0)$ and $z_1'(0)$, $z_2'(0)$, and $f'(z_0)$ are all non-zero. Then the angles between the curves $(z_1(t), z_2(t))$ and $(f(z_1(t)), f(z_2(t)))$ at $t = 0$ satisfy:*
$arg(z_2'(t)) - arg(z_1'(t))|_{t=0} = arg(f(z_2(t)))' - arg(f(z_1(t)))'|_{t=0} \, mod(2\pi)$ *[7]*

This theorem implies that conformal mappings locally preserve angles.

Theorem 3.3 (Riemann Mapping Theorem)**.** *Let $D \subset \mathbb{C}$ be a non-empty simply connected region. Then, there exists a bijective conformal map f which maps D onto the open unit disk ($\{z \in \mathbb{C} \,|\, |z| < 1\}$). This mapping is known as Riemann mapping and is unique provided that $f(z_0) = 0$ and $f'(z_0) > 0$, $\forall z_0 \in D$. [8]*

This is a powerful fact as analyticity places a strong constraint on a function, though the construction of the function is separate from the existence of it and may be extremely difficult.

Definition 3.4 (Riemann Surface)**.** A Riemann surface is a connected, Hausdorff topological space X equipped with an open covering U_i and a collection of homeomorphisms $f_i : U_i \to \mathbb{C}$ such that there exist analytic maps g_{ij} satisfying $f_i = g_{ij} \circ f_j$ on $U_{ij} = U_i \cap U_j$. [9]

Definition 3.5 (Conformal Equivalence)**.** Let U and V be two open sets in $\mathbb{C}$. U and V are conformally equivalent if there exists an analytic bijective function $f : U \to V$. f is called a conformal equivalence between U and V. [10]

Theorem 3.4 (Uniformisation Theorem)**.** *Let $D \subset \mathbb{C}$ be a simply connected Riemann surface. Then, D is conformally equivalent to one of the three Riemann surfaces: $\mathbb{C}$, the open unit disk, and the Riemann sphere. [11]*

This significantly generalises the Riemann mapping theorem in the context of Riemann surfaces.

3.2 Equations

3.2.1 Cauchy-Riemann Equations

Let $f(z) = u(x, y) + iv(x, y)$ where u and v are real functions of two variables $x, y \in \mathbb{R}$. Then, provided u and v are differentiable, f is holomorphic if and only if the partial derivatives of u and v satisfy the two equations:

$$\frac{\partial u}{\partial x} = \frac{\partial v}{\partial y} \quad (1) \quad \text{and} \quad \frac{\partial u}{\partial y} = -\frac{\partial v}{\partial x} \quad (2)$$

known as the Cauchy-Riemann equations. Real and imaginary parts of any conformal map together satisfy the Cauchy-Riemann equations. [12]

3.2.2 Laplace's Equation

If u and v satisfy the Cauchy-Riemann equations, then they also satisfy two dimensional Laplace's equation:

$$\nabla^2 F = \Delta F = \frac{\partial^2 F}{\partial x^2} + \frac{\partial^2 F}{\partial y^2} = 0$$

where ∇ is called the gradient operator, $\Delta = \nabla \cdot \nabla = \nabla^2$ is called the Laplace operator, and F is a twice-differentiable function of real values. [13] [14]

Real and imaginary parts of any conformal map each satisfies Laplace's equation. This is an extremely useful fact as Laplace's equation is known to be widely useful in the field of Mathematical Physics.

4 Fluid Flow

4.1 The Role of Conformal Mapping

Conformal mapping is a very useful tool when studying the flow of a fluid due to its preservation of harmonicity. Steady state fluid flows can be described by two harmonic functions that are defined later; the velocity potential and the stream function. After conformal mapping, these functions still remain valid, allowing for the study of more complex flows from simpler ones.

4.2 Background of External Fluid Flow

4.2.1 Underlying Assumptions

This chapter focuses particularly on external fluid flow, which describes the flow of an unbounded fluid over or around a body. The focus is on 2D steady fluid flow meaning that the flow is restricted to the (x,y) plane and is time invariant. We will assume that the fluid is "ideal", meaning it is [15]:

- Incompressible - the material density is constant within a fluid parcel.
- Irrotational - the vorticity of the fluid is equal to zero.
- Inviscid - the viscosity of the fluid is equal to zero.

Note: A model using these approximations is accurate only when the fluid is moving at subsonic speeds. As the speed approaches and exceeds mach 1 (speed of sound), shock waves appear in the fluid that are not considered/replicated by the model.
We will now introduce the velocity potential and stream function, which allow us to better understand the behaviour of a fluid as it flows.

4.2.2 Velocity Potential

Suppose there is a velocity field $\vec{V}$, then the vorticity $\vec{\omega}$ is defined as curl($\vec{V}$). By the irrotational flow assumption we have that:

$$\vec{\omega} = \nabla \times \vec{V} = \vec{0}$$

Now due to our assumptions, the velocity field can be represented as the gradient of a scalar function ϕ, i.e, $\vec{V} = \nabla\phi$, the above condition can be rewritten as:

$$\nabla \times \nabla\phi = \vec{0}$$

This condition is satisfied for all scalar functions ϕ, so this proves that there exists a scalar function such that $\vec{V} = \nabla\phi$ for irrotational flows and ϕ can now defined to be the velocity potential.
The continuity (in differential form) states:

$$\frac{\partial\rho}{\partial t} + \nabla \cdot (\rho\vec{V}) = 0$$

where ρ is fluid density and t is time.
By the assumption that our fluid is incompressible, the density is constant and so this allows the equation above to simply be expressed as:

$$\nabla \cdot \vec{V} = 0$$

Substituting $\vec{V} = \nabla\phi$ into this equation:

$$\nabla \cdot (\nabla\phi) = \nabla^2\phi = 0$$

This shows that the velocity potential satisfies Laplace's equation and so we can calculate it's harmonic conjugate ψ. This is known as the stream function. [16]

4.2.3 Stream Function

2D fluid flow can be visualised either through selecting a number of points and then drawing the corresponding flow velocity vectors at each point, or through streamlines, which are lines that show the paths that particles of fluid will take as the fluid flows. The advantage of streamlines can be seen in Figure 3 as it is much more clear to see how the fluid particles move.

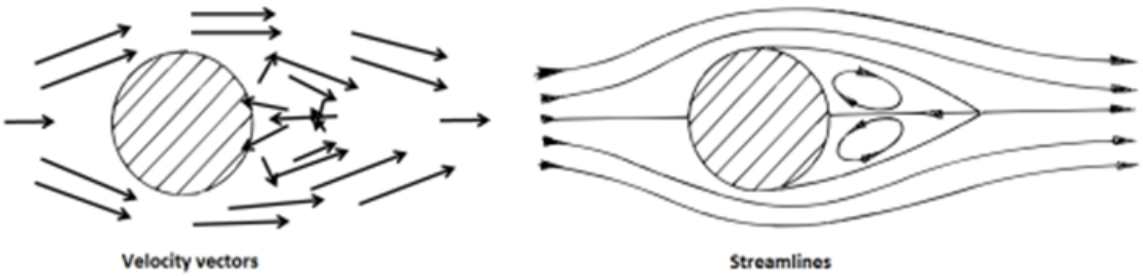

Figure 3: Diagrams giving a visual representation of fluid flow through flow velocity vectors and streamlines [17]

In 2D Cartesian coordinates, the stream function is a function of x and y, i.e:

$$\psi = \psi(x, y)$$

To obtain a single streamline, the stream function is equated to some constant $c \in \mathbb{R}$: [18]

$$\psi(x, y) = c$$

The equation above can be rearranged to obtain a function $y = y(x)$. The plot of this function gives the streamline corresponding to the constant c.
In order to obtain the desired streamlines, we need to find and plot each function $y = y(x)$ for different values of c. This family of curves are in fact the streamlines that can be used to visualise the fluid flow.

The stream function lets us find the components of the flow velocity $\vec{V} = a\hat{i} + b\hat{j}$ for the fluid.
Let a_p be the horizontal velocity component at any given point p. a_p can be obtained by computing the partial derivative of ψ in the y-direction and evaluating this at p, i.e:

$$a_p = \frac{\partial \psi}{\partial y}\bigg|_p$$

Similarly if b_p is the vertical velocity component at any given point p, then b_p can be calculated by computing

$$b_p = -\frac{\partial \psi}{\partial x}\bigg|_p$$

There is an alternative way to express the a and b components of the flow velocity $\vec{V}$, by finding the partial derivatives of ϕ and evaluating them at p. This is made clear through the Cauchy-Riemann Equations which tell us:

$$a_p = \frac{\partial \psi}{\partial y}\bigg|_p = \frac{\partial \phi}{\partial x}\bigg|_p \qquad \text{and} \qquad b_p = -\frac{\partial \psi}{\partial x}\bigg|_p = \frac{\partial \phi}{\partial y}\bigg|_p$$

With the velocity potential ϕ and the stream function ψ as stated above, define the complex potential function $F(z)$ as:

$$F(z) = \phi + i\psi \quad (3)$$

$F(z)$ is an analytic function that allows us to understand the behaviour of the fluid as it flows.

4.3 Interior Corner Flows

Interior corner flows is the study of fluids as they flow around corners of angle θ, where $\theta < \pi$. Figure 4 has diagrams which incorporate streamlines to show how a fluid would flow around the various types of corners.

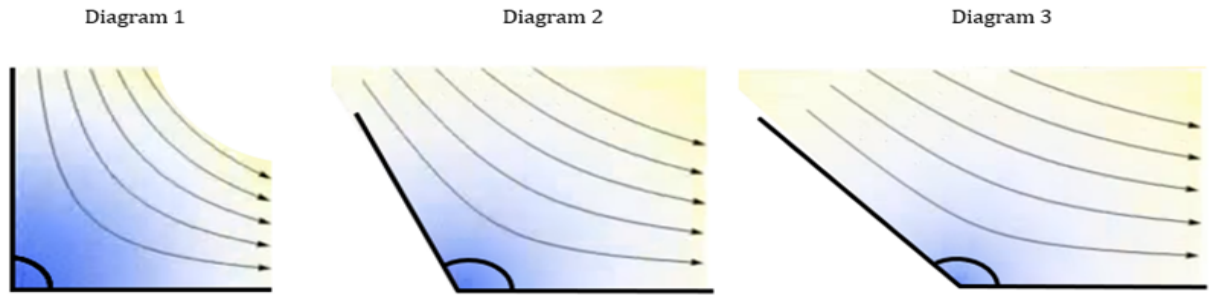

Figure 4: Diagrams showing fluid flows around interior corners with angles $\theta = \frac{\pi}{2}, \frac{2\pi}{3}$, and $\frac{3\pi}{4}$ respectively [19]

A particular use of fluid flow around a corner is seen in airflow around the corner of an air duct. This has applications in heating, ventilation, and air conditioning (HVAC) which is a very relevant aspect for most buildings. Airflow in a duct is generally not disrupted until the air has to pass a duct elbow, which is a right angle corner - thus it is important to understand fluid flow around this space. As a result, this is the case we will be focusing on in this report. [Diagram 1 in Figure 4]

4.3.1 The $w = z^2$ map

Consider the following conformal map:

$$w = g(z) = z^2$$

which has inverse

$$z = g^{-1}(w) = \sqrt{w}$$

The map $g(z)$ takes the first quadrant in the z-plane and maps it to the upper half-plane in the w-plane, while $g^{-1}(z)$ does the inverse and maps the upper half-plane back to the first quadrant. We can freely move back and forth between the first quadrant and upper half-plane as shown in Figure 2. [20]

4.3.2 Flow Around a Right Angle Corner

The method to find a flow solution for fluid flow around a right angle corner using conformal maps allows us to consider the much simpler scenario of straight fluid flow in the upper half-plane and then use the mapping $g(z)$ to obtain our desired flow solution. The behavior of the fluid in the two different domains can be visualised through Figure 5.

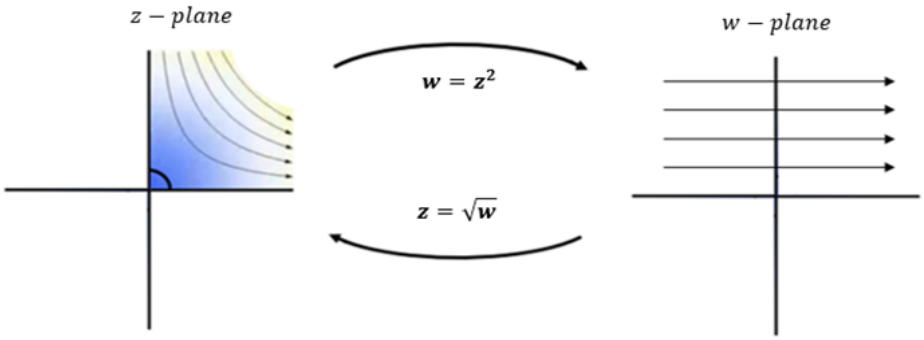

Figure 5: Geometric interpretation of the how the functions $g(z)$ and $g^{-1}(z)$ map the streamlines

For fluid flow in the upper half-plane (the w-plane in Figure 5), it is clear that the streamlines are parallel to the real axis, and so the stream function ψ must also be parallel to the real axis. For some $A \in \mathbb{R}$, this is satisfied by the following function:

$$\psi(x, y) = Ay$$

This is clear since equating this to some constant $c \in \mathbb{R}$ gives the equation:

$$\psi(x, y) = Ay = c$$

which can be rearranged to obtain the streamlines

$$y = y(x) = \frac{c}{A}$$

This clearly gives us a family of horizontal lines, which is exactly as required. This stream function is trivially harmonic, and so we can find its harmonic conjugate which will be the velocity potential of the flow. This is just Ax. Through this, the complex potential function (as introduced in equation (3)) for fluid flow in the upper half-plane can be written as:

$$F(z) = Az = Ax + iAy$$

Claim 4.1. If $\vec{V}$ is the velocity field and $F(z)$ is the complex potential function describing the flow of some fluid then:

$$\vec{V} = \overline{F'(z)}$$

Proof. We know $\vec{V} = \nabla\phi$ and we have that

$$\vec{V} = \nabla\phi = \frac{\partial\phi}{\partial x} + i\,\frac{\partial\phi}{\partial y}$$

We also know $F(z) = \phi + i\psi$, so we have that

$$F'(z) = \frac{\partial\phi}{\partial x} + i\,\frac{\partial\psi}{\partial x}$$

By the Cauchy-Riemann Equations,

$$F'(z) = \frac{\partial\phi}{\partial x} - i\,\frac{\partial\phi}{\partial y}$$

since

$$\frac{\partial\psi}{\partial x} = -\frac{\partial\phi}{\partial y}$$

Now consider the complex conjugate of $F'(z)$, which is

$$\overline{F'(z)} = \frac{\partial\phi}{\partial x} + i\,\frac{\partial\phi}{\partial y} = \nabla\phi = \vec{V}$$

□

It is clear that $F'(z) = A$, and using the fact that $\vec{V} = \overline{F'(z)}$ (where $\vec{V}$ is the velocity field):

$$\vec{V} = \overline{F'(z)} = \overline{A} = A = A + i0$$

This matches our geometric interpretation of fluid flow in the upper half-plane as $\vec{V} = A$ tells us that the fluid has constant horizontal velocity A and no vertical velocity everywhere.

Note: The direction of the flow depends on the sign of A, if $A > 0$ then the fluid will flow from left to right and if $A < 0$ then the fluid will flow in the opposite direction.

Since we have this complex potential function $F(w)$ in the w-plane (upper half-plane), the complex potential function in the z-plane (first quadrant) can be computed through the use of the conformal map $w = z^2$.

This function is given by:

$$F(g(z)) = F(z^2) = \phi + \psi = Az^2 = A((x+iy)^2) = A(x^2 - y^2) + i2Axy$$

where $A(x^2 - y^2)$ is the velocity potential and $2Axy$ is the stream function for the flow of a fluid around a right angle corner.

Consider the stream function $\psi(x, y) = 2Axy$. This function can be used to obtain the streamlines which indeed describe fluid flow around a right angle corner as initially desired. As from section 4.2.3, equate our stream function to some constant $c \in \mathbb{R}$ to obtain

$$\psi(x, y) = 2Axy = c$$

This can be rearranged to obtain

$$y(x) = \frac{c}{2Ax}$$

By varying the constant c and plotting each corresponding function, we obtain the following family of curves

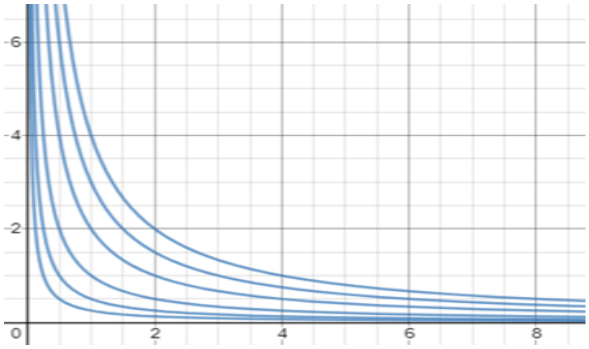

Figure 6: *Visual representation of the streamlines produced by the stream function obtained through conformal mapping*

This describes the way fluid flows around a right angle corner, as initially desired.

4.4 Flows Around an Airfoil

The cross section of any object designed to create lift can be called an airfoil. This includes any form of wing, fins, or propellers. The study of airfoils is therefore very useful for increasing the efficiency of transport and fluid propulsion. In 1910, the Russian mathematician Nikolai Zhukovsky published his work on the Joukowsky transform, a conformal map that can be used to model and study airfoils. This section uses this transform to model fluid flow around an airfoil and to estimate the lift coefficient of the NACA 23012 airfoil.

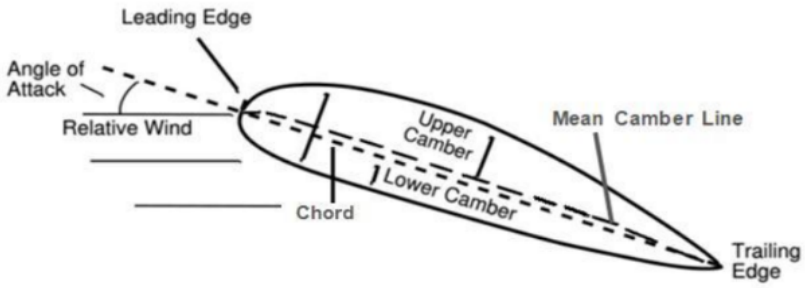

Figure 7: Diagram of the key properties of an airfoil [16]

Our model must satisfy the Kutta condition which is as followed: [21]

- The circulation takes a value such that the flow leaves the trailing edge smoothly for any given angle of attack.
- If the trailing edge is finite, then the velocity at the trailing edge must be zero.
- If the trailing edge is cusped, then the velocity at the trailing edge must be finite and parallel to the the upper and lower airfoil.

In nature, the Kutta condition is naturally followed due to the presence of friction from the upper and lower airfoil edges. When modelling an airfoil, we need to ensure that this property is reconstructed in the absence of friction. The flow around an airfoil can be found by mapping the superposition of three basic flows: Uniform flow, Doublet flow, and Vortex flow. [21]
These flows will all be presented in polar coordinates where:

$$z = x + iy = re^{i\theta}$$

4.4.1 Source/Sink Flow

A source flow is a flow where all streamlines are lines diverging from the origin. A sink flow is the opposite, where all streamlines are lines converging to the origin. The velocity potential and stream function for these flows are given by: [16]

$$\phi = \frac{K}{2\pi} \ln r$$

$$\psi = \frac{K}{2\pi} \theta$$

where $K \in \mathbb{R}$, $K > 0$ for a source flow, and $K < 0$ for a sink flow.

4.4.2 Uniform Flow

Consider the flow where all streamlines are straight parallel lines at an angle to the x-axis, θ. A uniform flow parallel to the x-axis can be regarded as the superposition of a source flow at minus infinity and a sink flow at plus infinity. The velocity potential and stream function for a uniform flow with velocity V_∞ at infinity are given by: [16]

$$\phi = V_\infty r \cos \theta$$

$$\psi = V_\infty r \sin \theta$$

4.4.3 Doublet Flow

The source and sink flow can also be used to create a doublet flow. Consider the resulting flow created when a source flow and a sink flow are separated by a distance $2d$. As $d \to 0$ a doublet flow forms. This is shown in Figure 8. The velocity potential and stream function for a doublet flow are given by: [16]

$$\phi = \frac{K}{2\pi} \frac{\cos \theta}{r}$$

$$\psi = -\frac{K}{2\pi} \frac{\sin \theta}{r}$$

where $K \in \mathbb{R}$.

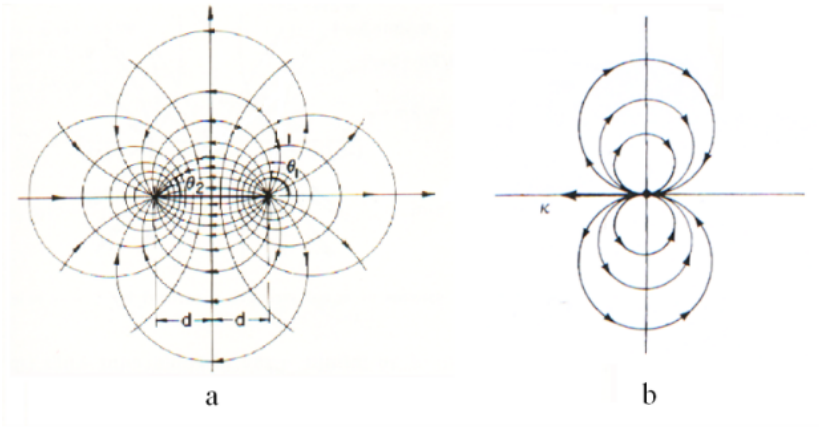

Figure 8: *(a) Source and sink flow at a distance of* $2d$*. (b) Doublet flow formed as* $d \to 0$ *[16]*

4.4.4 Vortex Flow

Consider the flow where all streamlines are concentric circles around the origin. This is a vortex flow. The velocity potential and stream function for a vortex flow are given by: [16]

$$\phi = -\frac{\Gamma\theta}{2\pi}$$

$$\psi = \frac{\Gamma}{2\pi}\ln r$$

where Γ is the strength of the vortex flow, also known as the circulation. As the stream function can be summed with an arbitrary constant, let

$$\psi = \frac{\Gamma}{2\pi}\ln r + c$$

where

$$c = -\frac{\Gamma}{2\pi}\ln R$$

where R is the radius of an arbitrary circle. This leaves the stream function as

$$\psi = \frac{\Gamma}{2\pi}\ln\frac{r}{R}$$

4.4.5 Flow Around a Cylinder

The flow around a cylinder can be represented as the superposition of a uniform, vortex and doublet flow. The resulting velocity potential and stream function are: [16]

$$\phi = V_\infty r\cos\theta - \frac{\Gamma\theta}{2\pi} + \frac{K}{2\pi}\frac{\cos\theta}{r}$$

$$\psi = V_\infty r\sin\theta + \frac{\Gamma}{2\pi}\ln\frac{r}{R} - \frac{K}{2\pi}\frac{\sin\theta}{r}$$

Set $K = 2\pi R^2 V_\infty$. From equation (3), the velocity potential and stream function of a cylinder of radius R centred at the origin can be written with complex potential:

$$F(z) = V_\infty(z + \frac{R^2}{z}) + i(\frac{\Gamma}{2\pi}\ln\frac{z}{R})$$

The mapping can be rotated by substituting $ze^{i\alpha}$ for z, giving

$$F(z) = V_\infty\left(ze^{i\alpha} + \frac{R^2e^{-i\alpha}}{z}\right) + i\left(\frac{\Gamma}{2\pi}\ln\frac{ze^{i\alpha}}{R}\right)$$

We can also recenter the circle by letting $z - z_0$ replace z. This leaves the complex potential as:

$$F(z) = V_\infty\left((z-z_0)e^{i\alpha} + \frac{R^2e^{-i\alpha}}{z-z_0}\right) + i\frac{\Gamma}{2\pi}\ln\left(\frac{(z-z_0)e^{i\alpha}}{R}\right)$$

4.4.6 Mapping to an Airfoil

To map a cylinder to an ellipse, the Joukowsky transformation

$$f(z) = z + \frac{\lambda^2}{z}$$

maps the circle of radius $r > \lambda$, centred at the origin onto the ellipse with semi-major axis $(r^2 + \lambda^2)/\lambda$ and semi-minor axis $(r^2 - \lambda^2)/\lambda$.

If the circle has center $x_0 + iy_0$ such that $|x_0 + iy_0| > 0$ then applying a Joukowsky transformation with $\lambda = x_0 - R\cos\beta$, where β is defined as angle between the x-axis and the line segment passing through the x-intercept and the cylinder center, will result in an airfoil. [22]

4.4.7 Circulation

As we will be considering an airfoil with a cusped trailing edge, the Kutta condition requires that when the angle of attack $\alpha = 0$ and $r = R$ the velocity is finite at $\theta = \beta$. When considering the velocity for an airfoil $\vec{V_a}$ you can use chain rule and calculate the velocity for a cylinder $\vec{V_c}$ multiplied by the derivative of the inverse transform:

$$\vec{V_a} = \vec{V_c} \cdot \left(1 - \frac{\lambda^2}{z^2}\right)^{-1}$$

We can see that if $z = \lambda$ the velocity on the cylinder is only finite when $\vec{V_c}$ is zero. To find Γ we can find the velocity of the cylinder in the θ direction by calculating the partial derivative of ϕ with respect to θ.

$$V_\theta = \frac{1}{r}\frac{\partial \phi}{\partial \theta} = V_\infty \sin\theta - \frac{\Gamma}{2\pi r} + \frac{K}{2\pi}\frac{\sin\theta}{r^2}$$

Setting $K = 2\pi R^2 V_\infty$ as above, $\theta = \beta$, $r = R$ leaves $2V_\infty \sin\beta - \frac{\Gamma}{2\pi R} = 0$. Rearranging for Γ and accounting for an angle of attack α gives: [16]

$$\Gamma = 4\pi V_\infty R \sin(\alpha + \beta)$$

4.4.8 Plotting the Streamlines of an Airfoil

The streamlines of the flow around an airfoil can be found and plotted by mapping the streamlines of the flow around the cylinder using the Joukowsky transformation.

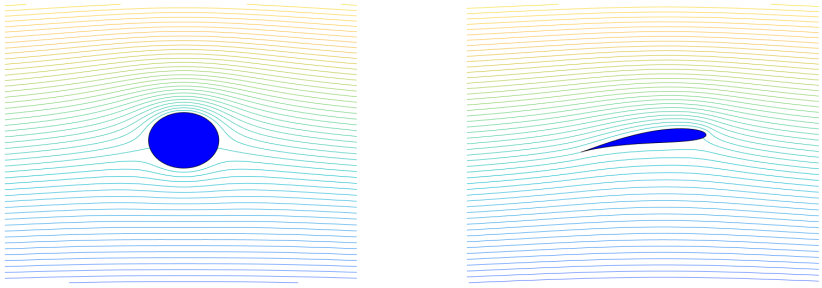

Figure 9: *Joukowsky transformation from a circle of radius $R = 1$ m centred at $x_0 = 0.1$ m $y_0 = 0.1$ m, with freestream velocity $V = 1ms^{-1}$ and angle of attack $\alpha = 10$*

4.4.9 Calculating the Lift Coefficient of the NACA 23012 Airfoil

This conformal mapping can also be used to estimate the lift coefficient of an actual airfoil. The Kutta-Joukowski theorem for an airfoil states that the lift per unit span can be found to be: [21]

$$L' = \rho V_\infty \Gamma$$

The lift coefficient can be calculated from this with c as the chord length of the airfoil as: [22]

$$C_L = \frac{2L'}{\rho {V_\infty}^2 c} = \frac{2\Gamma}{V_\infty c}$$

We will analyse the NACA 23012 airfoil, one of the most common airfoils of all time. [23] Using a trial and error method, the circle that gives the closest approximation to the airfoil after transforming is found.

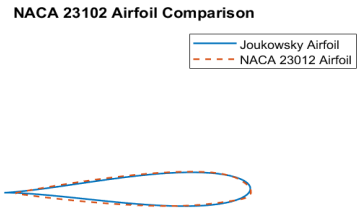

Figure 10: *NACA 23012 airfoil (red) compared to the Joukowsky airfoil created from a circle with radius* $R = 0.285$ *m and center at* $x_0 = 0.025$ *m,* $y_0 = 0.001$ *m, rotated* 1 *degree (blue) (The NACA 23012 airfoil was plotted with help from [24]*

To visualise the accuracy of our results we can plot the lift coefficient against the angle of attack from the Joukowsky transformation and the thin airfoil theory. The lift coefficient of the airfoil using the thin airfoil theory was found. [25]

From Figure 11 we can see that the lift coefficient predicted by the Jowkowsky airfoil is similar to the lift coefficient predicted by the thin airfoil theory, especially at a low angle of attack. Both methods also show that lift increases linearly with angle of attack.

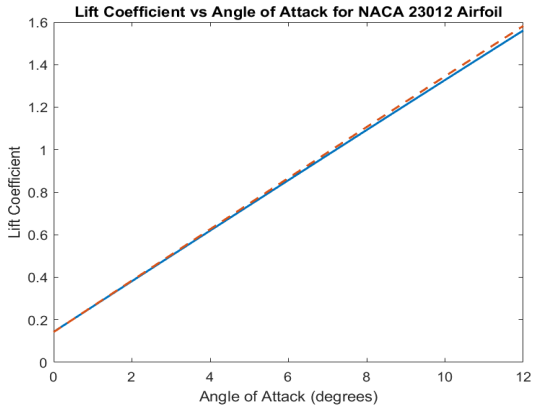

Figure 11: *Lift coefficient plotted against angle of attack for the Joukowsky airfoil (blue) compared to the thin airfoil (red)*

4.4.10 Error

The error of this method can be analysed from Figure 11. We see that the results agree to 1-3 decimal places, with the methods being more in agreement for lower angles of attack.

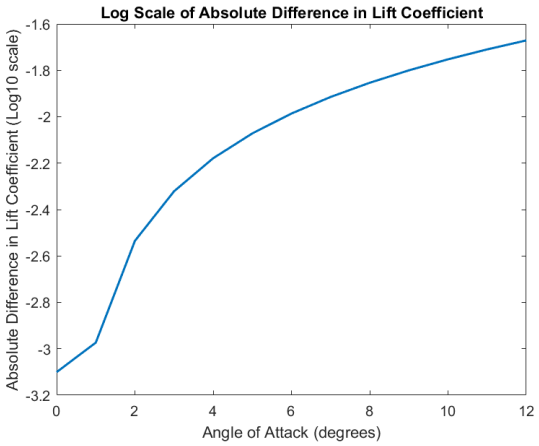

Figure 12: *Absolute value of the difference between the lift coefficient calculated using the Joukowsky airfoil method and the lift coefficient calculated using the thin airfoil theory*

Some of this error may be due to the difference between the airfoil shape created and the actual NACA 23012 airfoil. Another cause ofhttps://www.overleaf.com/project/5ed12b752150460001e6c48f error that will not be shown in the graph is that the thin airfoil theory will not have a completely accurate value for the lift coefficient due to it also being an approximation. Additionally, both methods also assume that the fluid is inviscid and incompressible which are unrealistic assumptions and will contribute to the overall error.

5 Medical Imaging

With technological advancements occurring continuously within the field of Medicine and Mathematics, experts have managed to successfully help bridge these two disciplines together within the world of medical imaging via computational conformal geometry to help with diagnoses. This chapter presents two different algorithmic methods to demonstrate how conformal geometry is applied via Virtual Colonoscopy:

- Method 1 computes the conformal structure of the colon surface, represented as a set of holomorphic 1-form basis.
- Method 2 uses Ricci flow method via a circle packing metric and uses the shape index SI to visualise the colon surface and ultimately guide a registration.

5.1 The Role of Conformal Mapping

Computational conformal geometry is a growing inter-disciplinary field between computer science and modern geometry; it is the study of the set of angle-preserving transformations- in particular, conformal maps.

The goal of computational conformal geometry is to convert concepts and theorems from Riemann surface theory to practical algorithms. Via the uniformisation theorem (Theorem 2.4), the key principle that allows us to apply conformal geometry is that the uniformization property can convert general 3D geometric problems to 2D problems in these canonical domains, which is essential in medical imaging, in order to analyse 3D anatomical structures. In general, conformal mapping algorithms can be classified - the following table breaks down the classification and their characteristics: [26] [27] [28]

Class	Method	Maps	Genus Surface Type
First	Computes surface to plane	Harmonic Maps, Least Squares Conformal Maps and Spherical Maps	Zero
Second	Computes derivatives of maps	Holomorphic forms	One
Third	Computes conformal metrics to induce conformal maps	Ricci Flow	Any

Table 1: Conformal Mapping Algorithms [28]

5.2 Background of Virtual Colonoscopy

Virtual colonoscopy has provided substantial evidence that it is more efficient and suited than the real optical colonoscopy, however, there are problems that still occur during examinations. Virtual colonoscopy (VC) uses a virtual fly-through visualization system and computed tomographic (CT) images of patient's abdomen - this guides physicians around a 3D model of the colon searching for polyps, the indicators of a potential cancer. [29]

5.3 Extra Topological Definitions

Before investigating the process of conformal colon flattening, we introduce some significant technical definitions: [30] [29] [31] [32]

Definition 5.1 (Genus)**.** The genus (handle) of an orientable surface (i.e. a surface that has a consistent surface normal vector at each point), is the number of *holes* it has.

Definition 5.2 (Manifold)**.** A manifold is a topological space that locally resembles Euclidean space near each point.

Definition 5.3 (Chart)**.** A chart (U, φ) for a topological space M is a homeomorphism φ from an open subset U of M to an open subset of an Euclidean space.

Definition 5.4 (Atlas)**.** An atlas is a family of charts,$(U_\alpha, \varphi_\alpha)$, where U_α constitutes an open covering of M.

Definition 5.5 (Homotopic)**.** Two closed curves are homotopic if they can deform to each other on the surface.

Definition 5.6 (Holomorphic 1-form)**.** Given a Riemann surface M with a conformal structure A, a holomorphic 1-form ω is a complex differential form, such that on each local chart $(U, \varphi) \in A$,

$$\omega = f(z)dz$$

where $f(z)$ is an analytic function; $z = u + iv$ is the local parameter in the complex form.

5.4 Method 1

In order to visualise polyps, we illustrate a clear and thorough technique, which is split up into 3 chronological ideas:

1. Topological Denoising
2. Conformal Colon Flattening
3. Direct Volume Rendering

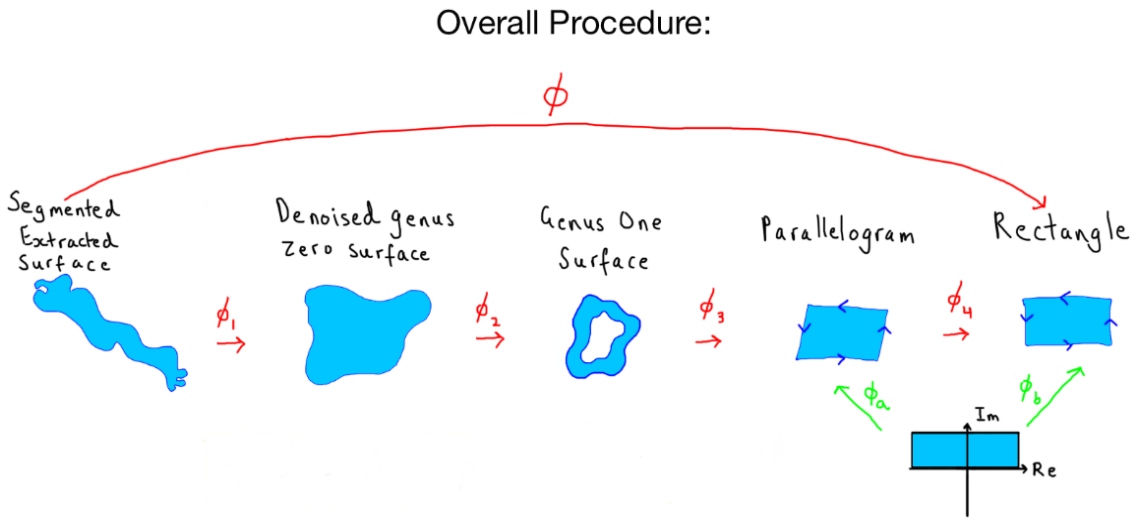

Figure 13: *Map composition illustrating the generation of a conformally mapped rectangle from a segmented extracted surface where* $\{\phi_i\}_{i=1}^4$ *are bijective conformal maps*

5.4.1 Topological Denoising

The segmented extracted colon surfaces from the CT scan have complex topologies caused by the inaccuracy of the reconstruction methods. This potentially causes additional *false* genus structures to the surface which can produce misleading representations of the organ. An arduous task therefore is to remove these *handles*. One procedure to identify them is locating the shortest loop for each homotopy class.

It is possible to deduce the shortest loop in each surface that contains *handles* M by translating this problem onto a universal covering space $\tilde{M}$ through a projection map π and looking for the shortest path. This problem was solved by Éric Colin de Verdière and Francis Lazarus. [33]

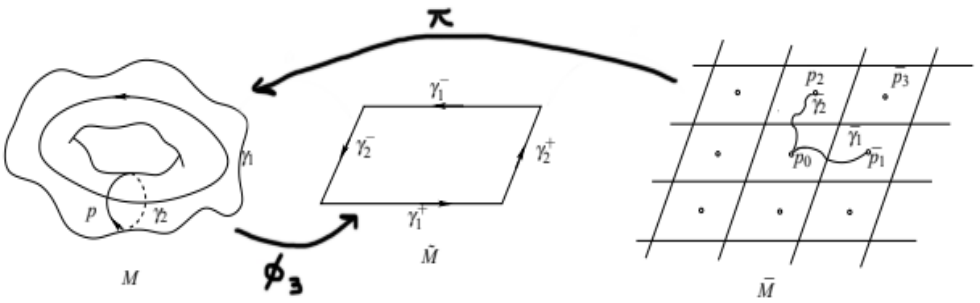

Figure 14: *Finding the shortest loop in the segmented extracted surface in M by calculating the shortest path in $\bar{M}$ by using the projection map π. Then, mapping surface M to a fundamental domain (rectangle) $\tilde{M}$* under ϕ_3. [29]

ϕ_1 maps the extracted segmented surface to a denoised genus-zero surface by locating and removing the topology noise (i.e. minute handle). [29]

5.4.2 Conformal Colon Flattening

The denoised genus-zero colon surface is then mapped to a 2D rectangle. This is done in the following: [29]

- ϕ_2: The denoised genus-zero surface is mapped to a genus-one surface by:
  - Computing the holomorphic 1-form on the 3D colon surface mesh via the conjugate gradient method and then cutting along a trajectory on the colon surface using the holomorphic 1-form.
  - Then a double covering method ensures a genus-one surface is formed. [Appendix]
- ϕ_3: Two curves γ_1, γ_2 on a surface M form a cut graph. M is sliced open along the cut graph to become a fundamental domain $\tilde{M}$, which forms a parallelogram. [Figure 14]
- ϕ_4: The parallelogram obtained is mapped to a rectangle via $\phi_b \circ \phi_a^{-1}$. ϕ_a and ϕ_b map an upper half-plane to a parallelogram and rectangle respectively, which can be constructed through Schwarz-Christoffel mapping. [Appendix]

Therefore the map from the segmented extracted surface to a *triangulated* rectangle ϕ can be established by composing the transformations related to topological denoising and conformal colon flattening:

$$\phi = \phi_4 \circ \phi_3 \circ \phi_2 \circ \phi_1$$

Riemann mapping theorem (Theorem 3.3) implies the existence of the bijective conformal map, ϕ. This process has now shown that ϕ can be constructed, which can then be used to recreated the 3D colon surface by rendering.

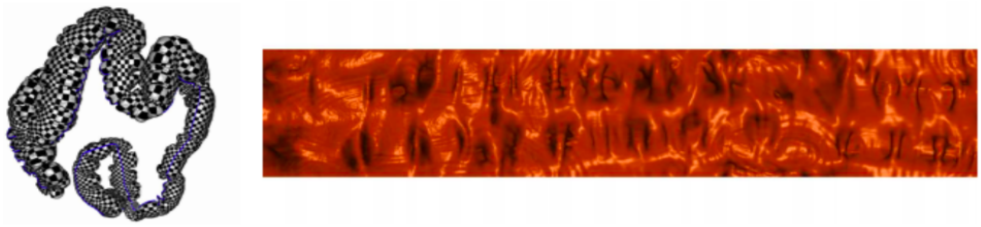

(a) Holomorphic 1-form (b) Conformal virtual colon flattening

Figure 15: *(a) Illustrates the holomorphic one-form on the colon surface by texture-mapping a checker board image. (b) Exhibits the conformal flattening induced by (a)* [29]

5.4.3 Direct Volume Rendering

This particular flattening algorithm leaves us with a triangulated rectangle - hence, the polyps are automatically flattened. A direct volume rendering method to render the flattened colon image is necessary for the detection of the polyps as it recreates the 3D colon surface from the 2D flattened image. It is carried out by camera registration, followed by volumetric ray casting.

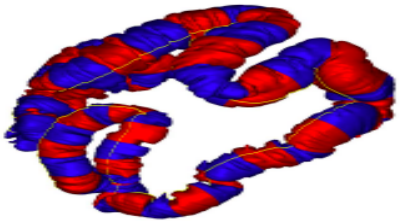

Figure 16: *Rendering process* [29]

Collating all these ideas together will lead to the eminent detection of polyps. [29]

5.4.4 Overview of Method 1

The following table summarises the advantages and disadvantages of this process:

Advantages	Disadvantages
The shortest loop algorithm automatically removes the topological noise	The denoising algorithm cannot always get a genus 0 surface
The conjugate descent method has a lower computational cost compared to the Newton method	The conjugate descent method is more complicated than the steepest descent method and is tailored for specific situations
Optimising and utilising the harmonic energy principle allows the global distortion from the colon surface to the rectangle to be minimised	Even though we know a ϕ exists, it is difficult to explicitly generate a ϕ

Table 2: Analysis of Method 1 [22] [24] [27] [28]

5.5 Ricci Flow

Ricci flow is a relatively new concept in Mathematics which became popular after being used to prove the Poincare conjecture by Grigori Perelman in 2006. This idea is now unexpectedly being used in medical imaging. Before investigating the process of how Ricci flow is implemented in VC, we introduce some significant mathematical definitions:

Definition 5.7 (Riemannian Metric)**.** Riemannian metric defines lengths of vectors and curves in a manifold. Suppose for every point x in a manifold M, an inner product $< \cdot, \cdot >_x$ is defined on a tangent space T_xM of M at x. Then the collection of all these inner products is called the Riemannian metric. [34]

Definition 5.8 (Gaussian curvature)**.** Let κ_1 and κ_2 be the principal curvatures of a surface patch σ. The Gaussian curvature K of σ is the product of κ_1 and κ_2: $K = \kappa_1\kappa_2$ [35]

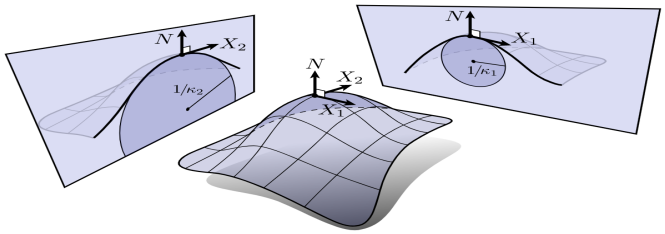

Figure 17: *Gaussian curvature representation* [36]

Ricci flow is the process of deforming the Riemannian metric of the surface. The rate of this deformation is proportional to the Gaussian curvature such that the curvature evolves like a non-linear heat diffusion. The rate of change of Riemannian metric is represented by: [37]

$$\frac{dg_{ij}(t)}{dt} = -2K(t)g_{ij}(t)$$

where $K(t)$ is the Gaussian curvature and $g_{ij}(t)$ is Riemannian metric, both as functions of time t.
The curvature flow is represented as:

$$\frac{dK(t)}{dt} = \Delta_{g(t)} + 2K^2(t)$$

where $\Delta_{g(t)}$ is the Laplace–Beltrami operator induced by the metric $g(t)$.

Hamilton and Chow proved that during the flow, the curvature $K(t)$ is always finite, never blows up, and when time goes to infinity, it converges to a constant: $K(t) \to constant$ as $t \to \infty$. Therefore, the 3D object with Gaussian curvatures for Ricci flow can be classified into three categories depending on the sign of K.

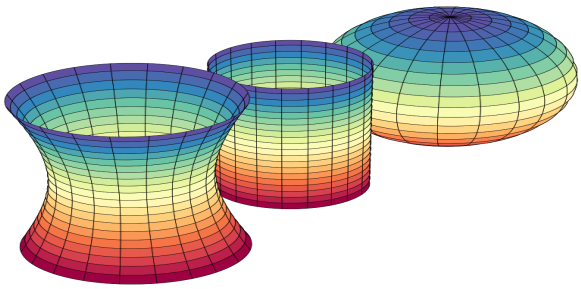

Figure 18: *Gaussian curvatures with* $K < 0$, $K = 0$, *and* $K > 0$ [38]

5.6 Method 2

An alternative method to detect polyps is to take two images of the patient's colon from prone and supine scans of the patient. This is to reduce the chance of false positive diagnoses. Succinctly, Method 2 reformulates the conformal mapping of the inner colon surface to a cylinder for the application of prone and supine registration to replace current methodologies. A positive diagnosis is only given when both the 2D images (that are obtained when transforming the 3D images) agree with the presence of a polyp structure. [39]

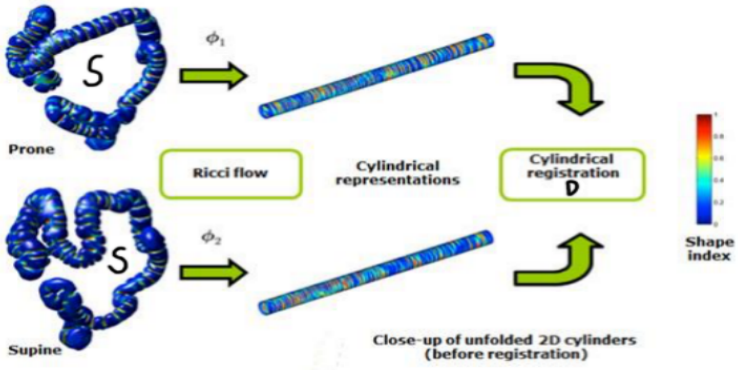

Figure 19: *Mapping process of inner colon surface to the plane where the colour scale indicates the shape index (SI) and* ϕ *is a conformal map* [39]

Note: The Ricci flow in this context is also known as the gradient flow of the Ricci energy. This can be minimised using the steepest gradient descent method.

5.6.1 Parameterisation of the Inner Colon Surface

The parameterisation is defined here by:

$$\frac{du_i(t)}{dt} = \bar{K}_i - K_i$$

where u_i each corresponds to a radius calculated from a circle packing metric, $\bar{K}_i \in \mathbb{R}$ is the desired Gaussian curvature, and $K_i \in \mathbb{R}$ is the local discrete Gaussian curvature of an inner colon S. For a surface with a cylinder topology such as the colon, the resulting Gaussian curvature function is zero everywhere. So, in order to produce the map onto the plane, set $\bar{K}_i$ to zero at all vertices.

Note: In order to parameterise S with the Ricci flow method, S is converted into a genus-one surface using a double-covering method. [39]

5.6.2 Inner Colon Surface Extraction

The inner colon surface is extracted by using the segmentation of air inside the colon. To ensure that the surfaces are all genus-zero, the segmentations are manually edited. The discrete surface mesh is then extracted applying the marching cubes algorithm. The Ricci flow method allows the mesh to be smoothed to obtain a convergent, continuous surface. Finally, in order to fully define the ϕ map, a quadratic edge collapse method and Loop-subdivision method are used respectively which reduces computational time. [39]

5.6.3 Cylindrical Representation of the Inner Colon Surface

Another step before getting the final rectangle plane D is to minimise the $E_{max} = \bar{K}_i - K_i$ using Ricci flow. The following picture gives a visualisation: [39]

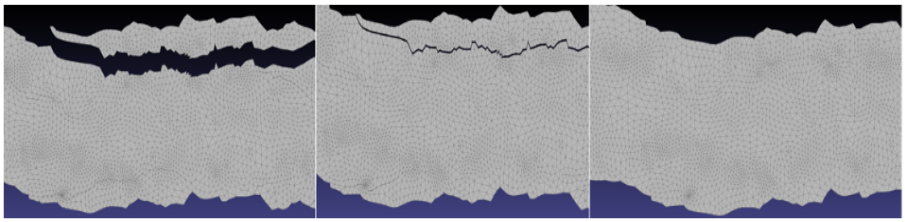

Figure 20: Planar Graphs with the value of E_{max} decreasing from left to right [39]

The surface embedding process is iterative and starts with one face and adding nearby surfaces repeatedly. However, gaps and overlaps of faces may be present at this stage due to the fact that K_i may not be exactly zero at every vertex. This can be dealt with by reducing the E_{max} by Ricci flow.
Finally, the Ricci flow process is stopped when E_{max} is small enough. Although the final picture is not a rectangle, it can be transformed into one. The last picture shows the alignment of the resulting rectangles from the prone and supine images. Shape index (SI) is implemented to represent anatomical features, where $SI = \frac{1}{2} - \frac{1}{\pi}\arctan\left(\frac{\kappa_1+\kappa_2}{\kappa_1-\kappa_2}\right)$ where κ_1 and κ_2 are the principal curvatures of $\sigma(u, v)$. [35]

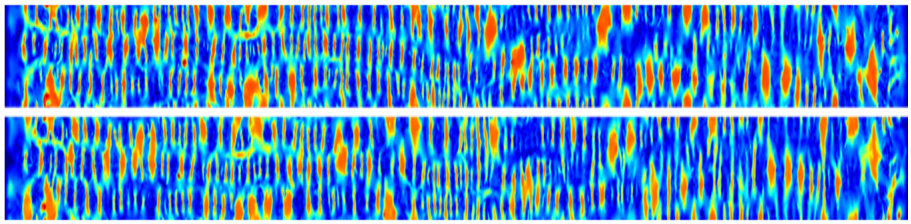

Figure 21: *Prone and supine images of the inner colon surface with the shape index as intensity.* [39]

5.6.4 Overview of Method 2

The following table summarises the advantages and disadvantages of this process:

Advantages	Disadvantages
Ricci flow method shares most of the positives from Method 1 but additionally can handle arbitrary topological objects and has fewer algorithmic steps so can be generalised to more scenarios e.g. Brain Surface Mapping, Facial Recognition etc...	Marching cubes algorithm can create meshes which are highly over-sampled hence there are massive usage problems
The use of isothermal co-ordinates allows for better global surface parameterisation	Inconsistent choices for neighbouring cubes in marching cubes algorithm can lead to extra holes being created which slows down the process
The Discrete Ricci flow computation is fully parallelisable due to the Marching Cube algorithm	The steepest descent method to minimise Ricci energy is very slow compared to conjugate descent and is not invariant by calculating the first order derivative

Table 3: Analysis of Method 2 [32] [33] [34]

6 Conclusion

6.1 Further Work

We can extend the Fluid Flow section by weakening the assumptions used since incompressible, inviscid, and irrotational fluid flow is rarely achieved in real world scenarios although it is much simpler to deal with. Easing the irrotational assumption means we can have a non-zero vorticity which will allow for turbulent flow to occur. We can then begin to look at how this disrupts fluid flow in general and then relate it to the important example of airflow in ducts. We can go on to see how we can minimise the dynamical losses caused by airflow in a duct elbow by optimising duct elbow shapes and through the use of turning vanes. For airfoils, modelling the fluid as a real viscous fluid and considering the effect of drag would provide a more realistic result. Unfortunately, this method does requires a higher degree of mathematical complexity and understanding but is used to great effect worldwide as it can then be used to optimise uses of airfoils such as increasing both fuel efficiency in airplanes and thrust from propellers.

Most of the review and research of VC application in this report has been obtained by David XiangFeng Gu's team (from Stony Brook University) which shows how modern this application of conformal geometry is, and that there is still a long way to go in seeing how current methods can be either numerically optimised or modelled better. We can for example look into other optimising algorithms to ensure that the denoising process (Method 1) can always generate a genus-zero surface. Also, we can use a metric other than circle packing (Method 2) to generate a more tangible discrete surface mesh in order to map the colon surface.

6.2 Evaluation

Having studied the applications of conformal mappings in Fluid Flow and Medical Imaging - two fields that are on different ends of the scientific spectrum - we have seen the crucial role it has played in the simplification of a variety of difficult 3D geometrical problems.

Two maps have been discussed in Fluid Flow, each dealing with completely different domains but both working to achieve the same goal: to remodel a problem by mapping from the given domain to a simplified one, finding the flow solution, then mapping it back to obtain the solution in the required domain. This method relies on both the invariance of harmonicity and the preservation of angles under conformal mapping.

Numerous existing methodologies to carry out VC, which incorporate different algorithms, have already been discussed in Medical Imaging and each attempt has been developed and improved upon. These two methods identically use the tool of conformal mapping to achieve the same outcome but in different ways so complement each other very well. The methods rely on conformal mappings to preserve angles and therefore local shapes - this allows polyps to be detected and visualised accurately on a 2D surface from a 3D surface.

Even though this report focused on the applications in Fluid Flow and Medical Imaging, it is also worth mentioning that the idea of conformal mapping can be extended to many other topics including: Electromagnetic Field, Acoustic, and Elasticity. The important properties of conformal mapping: invariance of harmonicity (Theorem 3.1) and preservation of angles (Theorem 3.2) explain the endless possibilities of applications of conformal mappings.

7 Appendix

7.1 Maps

A Schwarz-Christoffell transformation, named after Elwin Bruno Christoffel and Hermann Amandus Schwarz, is a family of conformal mappings which map the upper half-plane $\{\zeta \in \mathbb{C} \mid im(\zeta) > 0\}$ onto the interior of a polygon. Let P $\in \mathbb{C}$ be a polygon with n vertices. The Riemann Mapping Theorem implies that there exists a Riemann mapping f from the upper half-plane to the interior of P. Let $\alpha_1, \alpha_2, ..., \alpha_n$ be the interior angles of the n-polygon. Then the Riemann mapping is given by:

$$f(\zeta) = \int^{\zeta} \frac{K}{(z-x_1)^{1-\frac{\alpha_1}{\pi}}(z-x_2)^{1-\frac{\alpha_2}{\pi}} \dots (z-x_n)^{1-\frac{\alpha_n}{\pi}}} dz$$

$$\frac{dz}{d\zeta} = K(\zeta - x_1)^{\frac{\alpha_1}{\pi}-1)}(\zeta - x_2)^{(\frac{\alpha_2}{\pi}-1)} \dots (\zeta - x_n)^{(\frac{\alpha_n}{\pi}-1)}$$

where $K \in \mathbb{R}$, and $x_1 < x_2 < \cdots < x_n \in \mathbb{R}$ are values along the real axis of the ζ-plane, which each gets mapped onto a vertex of the polygon P in the z-plane. Any transformation which follows either of the forms is called a Schwarz-Christoffel transformation.

[40]

7.2 Algorithms

7.2.1 Noise Removing

After computing a homology basis $\{\gamma_1, \gamma_2, \cdots, \gamma_{2g}\}$ of M, its shortest homology basis $\{\gamma_1', \gamma_2', \cdots, \gamma_{2g}'\}$ can be computed. Each handle of M corresponds to two loops. A topology noise (i.e. minute handle) has a loop with very small length. Topology noise is removed by using the following algorithm: [29]

1. Compute the shortest homology basis $\{\gamma_1', \gamma_2', \cdots, \gamma_{2g}'\}$ of M.
2. Select $\{\gamma'\}$from the basis with the minimal length.
3. Slice M along γ, to get two boundary curves γ^+ and γ^-.
4. Fill γ^+ by a polygon, fill γ^- by a polygon, triangulate the filled mesh to get the resulting mesh $\tilde{M}$.
5. Repeat 2 through 4, until no minute handles are left.

[29]

7.2.2 Double Covering Method

1. Make a copy of mesh M, denoted as M', such that M' has all verticies in M, if $[v_0, v_1, v_2]$ is a face in M, then $[v_1, v_0, v_2]$ is a face of M'.

2. Glue M and M' along their boundaries, if a halfedge $[v_0, v_1]$ is on the boundary of M $[v_0, v_1] \in \partial M$, then $[v_1, v_0]$ is on the boundary of M'. Glue $[v_0, v_1]$ with $[v_1, v_0]$.

[29]

7.2.3 Conformal Parameterisation to a Parallelogram

Suppose $\{\omega_1, \omega_2, \ldots, \omega_g\}$ is a basis for $\Omega(M)$, where g is a genus of M. We can find a collection of open disks $U_\alpha \subset M$, such that U_α form an open covering of M, $M \subset \cup U_\alpha$. We define $\phi_\alpha^k : U_\alpha \to \mathbb{C}$ using the following formula, first we fix a base point $p \in U_\alpha$, for any point $q \in U_\alpha$,

$$\phi_\alpha^k(q) = \int_\gamma \omega_k$$

where the path $\gamma : [0, 1] \to U_\alpha$ is arbitrary curve connecting p and q and inside U_α, $\gamma \subset U_\alpha$, $\gamma(0) = p$, $\gamma(1) = q$. It can be verified that, we can select a ϕ_α^k, $k = 1, 2, \ldots, g$, such that ϕ_α^k is a bijection, we simply denote it as ϕ_α. Then, the atlas $\{(U_\alpha, \phi_\alpha^k)\}$ is a conformal atlas.

For a genus-one closed surface M, given a holomorphic 1-form $\omega \in \Omega(M)$, we can find 2 special curves $\Gamma = \gamma_1 \cup \gamma_2$, such that $\tilde{M}' = M/\Gamma$ is a topological disk. Furthermore, on each open set U_α, if the curve $\int_{\gamma_1} \omega$ is a horizontal line in the parameter plane, then γ_1 is a *horizontal trajectory*. We choose γ_2 such that $\int_{\gamma_2} \omega$ is a vertical line in the parameter plane, namely, γ_2 is a vertical trajectory. Γ is called a *cut graph*. Then by integrating ω on $\tilde{M}'$, $\tilde{M}'$ is conformally mapped to a parallelogram $\tilde{M}$.

[29]

7.3 MATLAB Code

The code below was developed by Tom Goacher using the method described in section 4.4.8.

7.3.1 Plotting the Streamlines

```
function streamlines(x0,y0,alpha,R,V)
%Inputs
%Centre of circle
%angle of the velocity of the freestream fluid with respect to the x axis
%Radius
%Velocity of freestream

%Convert alpha to radians
alpha = alpha*(pi/180);

%set the center of the circle
c = x0+1i*y0;

%angle between the x axis and the line segment from the x-intercept to the
    cylinder center
beta = atan(y0/sqrt(R^2-y0^2));

%define lambda
lambda = x0 - R*cos(beta);

%Creating a 2 dimentional array for values of Z
x = -10:0.05:10;
y = -10:0.05:10;
[X,Y] = meshgrid(x,y);
Z = X + 1i*Y;

%Removing points inside the circle
for j = 1:length(x)
```

```
    for k = 1:length(y)
        if abs(Z(j,k)-c) <=  R - 0.1
            Z(j,k) = NaN;
        end
    end
end

%Mapping the Z points using the Joukowsky transformation and rotating to
%keep the flow level when plotting
W = Z + lambda^2./Z;
W = W*exp(1i*alpha);

%Calculating the circulation around the cylinder
circ = 4*pi*V*R*sin(alpha+beta);
%Calculating the complex potential
f = V*((Z-c)*exp(1i*alpha)+exp(-1i*alpha)*R^2./(Z-c)) + 1i*(circ/(2*pi))*
   log((Z-c)*exp(1i*alpha)/R);

%plotting the mapped contour lines
figure(3)
contour(real(W),imag(W),imag(f),-7:0.2:7)
hold on

%Plotting the airfoil
theta = 0:pi/36:2*pi;
z = c+R*exp(1i*theta);
w = z + lambda^2./z;
w = w*exp(1i*alpha);
fill(real(w),imag(w),'b')

xlim([-5 5])
ylim([-5 5])
```

```
set(gca,'visible','off')
set(gca,'xtick',[])
hold off

%plotting the contour lines for the cylinder
figure(2)
Zc = X + 1i*Y;
Zc = Zc*exp(1i*alpha);
contour(real(Zc),imag(Zc),imag(f),-7:0.2:7)
hold on

%Plotting the circle
theta = 0:pi/36:2*pi;
z = c+R*exp(1i*theta);
z=z*exp(1i*alpha);
w = z + lambda^2./z;
fill(real(z),imag(z),'b')

xlim([-5 5])
ylim([-5 5])
set(gca,'visible','off')
set(gca,'xtick',[])
hold off

end
```

7.3.2 Comparing the NACA 23012 and Joukowsky airfoil

```
function AirfoilComparison(x0,y0,alpha,r)
%set the center of the circle
c=x0+1i*y0;

%Convert alpha to radians
alpha = alpha*(pi/180);
```

```
7
8  %define lambda
9  lambda = r-c;
10
11 %plot the joukowsky airfoil
12 theta = 0:pi/36:2*pi;
13 z = c + r*exp(1i*theta);
14 w = -0.03+0.009*1i+exp(1i*alpha)*(z + lambda^2./z);
15 plot(w,'LineWidth',1.2)
16 hold on
17
18 %plot the NACA 23012 airfoil
19 T = readtable('NACA.txt');
20 X = table2array(T(:,1))';
21 Y = table2array(T(:,2))';
22 plot(0.5-X,Y,'--','LineWidth',1.2)
23 xlim([-1 1])
24 ylim([-0.6 0.6])
25 end
```

7.3.3 Plotting the Lift Coefficient

```
1  function PlottingLiftCoeff(x0,y0,theta,R)
2
3  %set the center of the circle
4  c=x0+1i*y0;
5
6  %define lambda
7  lambda = R-c;
8
9  %Set V as an arbritary constant
10 V=1;
11
12 %define alpha and beta
```

```
13 alpha = 0:pi/180:12*pi/180;
14 beta = atan(y0/sqrt(R^2-y0^2));
15
16 %Calculate chord length
17 z1 = R+c;
18 z2 = -R+c;
19 w1 = z1+lambda^2/z1;
20 w2 = z2+lambda^2/z2;
21 chord = abs(w1-w2);
22
23 %Calculate Gamma
24 Gamma = 4*pi*V*R*sin(alpha+(beta+theta*pi/180)*ones(1,13));
25
26 %Lift coefficient for the joukowsky
27 lcJOW = 2*Gamma./(V*chord);
28
29 %Calculate the lift coefficient for the NACA 23012 using thin airfoil [
       REFERENCE]
30 T = readtable('NACA.txt');
31 X = table2array(T(:,1))';
32 Y = table2array(T(:,2))';
33 for i = 1:length(alpha)
34     [lcTHIN(i),~] = ThinAirfoil(X,Y,alpha(i)*180/pi);
35 end
36
37 %Plot the lift coefficients
38 plot((180/pi)*alpha,lcJOW,'LineWidth',1.5)
39 hold on
40 plot((180/pi)*alpha,lcTHIN,'--','LineWidth',1.5)
41 hold off
42 title('Lift Coefficient vs Angle of Attack for NACA 23012 Airfoil')
43 xlabel('Angle of Attack (degrees)')
```

```
ylabel('Lift Coefficient')

%Plot the absolute difference on a log scale
figure(2)
plot((180/pi)*alpha,log10(abs(lcJOW-lcTHIN)),'LineWidth',1.5)
title('Log Scale of Absolute Difference in Lift Coefficient')
xlabel('Angle of Attack (degrees)')
ylabel('Absolute Difference in Lift Coefficient (Log10 scale)')
end
```

References

1. Kythe, P. *Handbook of Conformal Mappings and Applications* ISBN: 978-1138748477 (Chapman and Hall/CRC, 2019).
2. Kythe, P. *Computational Conformal Mapping* ISBN: 978-1-4612-2002-2 (Birkhäuser, Boston, MA, 1998).
3. Laptev, A. *MATH95007 COMPLEX ANALYSIS 2020, LECTURES 26 27, EVALUATION OF DEFINITE INTEGRALS* University Lecture. 2020.
4. Analytic function. http://encyclopediaofmath.org/index.php?title=Analytic_function&oldid=3248. (accessed: 5.6.2020).
5. Laptev, A. *MATH95007 COMPLEX ANALYSIS 2020, LECTURES 6, HARMONIC FUNCTIONS* University Lecture. 2020.
6. Laptev, A. *MATH95007 COMPLEX ANALYSIS 2020, LECTURES 29 30, CONFORMAL MAPPINGS* University Lecture. 2020.
7. Laptev, A. *MATH95007 COMPLEX ANALYSIS 2020, LECTURES 26 27, EVALUATION OF DEFINITE INTEGRALS* University Lecture. 2020.
8. Krantz, S. G. *Handbook of Complex Variables* 86–87. ISBN: 0817640118 (Birkhäuser, Boston, MA, 1999).
9. McMullen, C. *Complex Analysis on Riemann Surfaces*
10. Smith, H. *Lecture 23: Conformal Equivalences* University Lecture. 2020.
11. Donaldson, S. *Riemann Surfaces* 117. ISBN: 9780198526391 (Oxford University Press, 2011).
12. Weisstein & W, E. *Cauchy-Riemann Equations* https://mathworld.wolfram.com/Cauchy-RiemannEquations.html.
13. Hosch, W. L. *Laplace's equation* https://www.britannica.com/science/Laplaces-equation.
14. Laptev, A. *MATH95007 COMPLEX ANALYSIS 2020, LECTURES 6, HARMONIC FUNCTIONS* University Lecture. 2020.
15. *Marine Hydrodynamics, Chapter 3 – Ideal Fluid Flow* University Lecture. https://ocw.mit.edu/courses/mechanical-engineering/2-20-marine-hydrodynamics-13-021-spring-2005/lecture-notes/lecture7.pdf.
16. Kapania, N. R., Terracciano, K. & Taylor, S. *Modeling the Fluid Flow around Airfoils Using Conformal Mapping* 2008.

17. Chernyshenko, S. & Gouder, K. *Introduction to Fluid Dynamics* University Lecture. https://www.imperial.ac.uk/media/imperial-college/faculty-of-engineering/aeronautics/msc/Intro.-to-Fluid-Dynamics,-2019-20.pdf.

18. Diersch, H.-J. G. *Streamline Computations Available in FEFLOW* http://www.feflow.info/fileadmin/FEFLOW/download/other_docs/streamlines.pdf.

19. Bradley, M. *Fluid Flow around a Corner* http://demonstrations.wolfram.com/FluidFlowAroundACorner/.

20. Crowdy, D. G. *The Geometry of Functions, and How to Use It* 2020.

21. John D. Anderson, J. *Fundamentals of Aerodynamics* Fifth. ISBN: 978-0-07-339810-5 (McGraw-Hill, 2008).

22. Brennen, C. E. *INTERNET BOOK ON FLUID DYNAMICS* http://brennen.caltech.edu/fluidbook/.

23. Garrison, P. *Airfoils: A Short History* 2009. https://www.flyingmag.com/technicalities/technicalities-short-history-airfoils/#:~:text=Possibly%20the%20most%20widely%20used,NACA%20Langley%20researcher%20Eastman%20Jacobs.

24. *NACA 23012 12% - NACA 23012 airfoil* http://airfoiltools.com/airfoil/details?airfoil=naca23012-il.

25. Atyya, M. *Solution of the boundary layer over an airfoil section* https://www.mathworks.com/matlabcentral/fileexchange/58130-solution-of-the-boundary-layer-over-an-airfoil-section. (accessed: 10.6.2020).

26. *Conformal geometry* https://en.wikipedia.org/wiki/Conformal_geometry.

27. Gu, D. X. *David Xianfeng Gu's Home Page* https://www3.cs.stonybrook.edu/~gu/.

28. Gu, X. *et al.* Ricci Flow for 3D Shape Analysis. https://www.cs.cmu.edu/~wangy/paper/iccv07-ricci.pdf. (accessed: 9.6.2020).

29. Hong, W., Gu, X., Qiu, F., Jin, M. & Kaufman, A. Conformal Virtual Colon Flattening. https://www.researchgate.net/publication/221115617_Conformal_Virtual_Colon_Flattening. (accessed: 7.6.2020).

30. *Genus (mathematics)* https://en.wikipedia.org/wiki/Genus_(mathematics)#:~:text=In%20mathematics%2C%20genus%20(plural%20genera,a%20torus%20has%20genus%201..

31. Xu, M. Conformal Mesh. http://www.math.udel.edu/~mou/students/Documentation_ConformalMesh-2010-Min.pdf (2010). (accessed: 5.6.2020).

32. *Lecture 9 - Riemannian metrics* Lecture. https://maths-people.anu.edu.au/~andrews/DG/DG_chap9.pdf.

33. De Verdière, É. C. & Liang, F. L. Optimal System of Loops on an Orientable Surface. https://graphics.stanford.edu/courses/cs468-03-winter/Papers/verdiere-lazarus.pdf (2002). (accessed: 10.6.2020).

34. Weisstein & W, E. *Riemannian Metric* https://mathworld.wolfram.com/RiemannianMetric.html.

35. Jia, Y.-B. Gaussian and Mean Curvatures. http://web.cs.iastate.edu/~cs577/handouts/gaussian-curvature.pdf (2019). (accessed: 9.6.2020).

36. Crane, K. *A Quick and Dirty Introduction to the Curvature of Surfaces* http://wordpress.discretization.de/geometryprocessingandapplicationsws19/a-quick-and-dirty-introduction-to-the-curvature-of-surfaces/.

37. Wei Zeng, X. D. G. *Ricci Flow for Shape Analysis and Surface Registration: Theories, Algorithms and Applications* 4. ISBN: 978-1-4614-8781-4 (Springer, 2013).

38. Nicoguaro. *Gaussian Curvature* https://en.wikipedia.org/wiki/Gaussian_curvature#/media/File:Gaussian_curvature.svg.

39. Roth, H. *et al.* Conformal Mapping of the Inner Colon Surface to a Cylinder for the Application of Prone to Supine Registration. http://www.bmva.org/miua/2010/miua-10-31.pdf. (accessed: 8.6.2020).

40. *Schwarz–Christoffel mapping* https://en.wikipedia.org/wiki/Schwarz%E2%80%93Christoffel_mapping.